IEEE Robotics and Automation Letters (RAL) paper presented at
2024 IEEE/RSJ International Conference on Intelligent Robots and Systems (IROS)
October 14-18, 2024. Abu Dhabi, UAE

Novel Design of a Pneumatic Longitudinal Actuator for Both Extending and Contracting Motions

Yasuka Tago[1], Yuki Satake[2], *Student Member, IEEE*, and Hiroyuki Ishii[3], *Member, IEEE*

***Abstract*—Various types of extendable and contractible soft actuators have been developed by utilizing their strength, lightweight, and flexibility. Most soft actuators focus on either the extending or contracting motion. In this study, we aim to achieve both motions in a single actuator. We propose a novel lightweight soft extendible actuator driven solely by air. Driven in low pressure, this actuator exhibits a high contraction rate and extends without the aid of any external force, such as gravity, and contracts under tension loads. The actuator weighed 191 g and realized a maximum length of 980 mm at extension and contraction rates of 870%. We experimentally evaluated the performance of the actuator with respect to the operating parameters and internal pressure during the extending motion and with respect to the exhaust air volume and contraction rate during the contracting motion under the application of a contraction force. The results indicate that the actuation principle can effectively prevent buckling. Additionally, an efficient contracting motion can be achieved as the contraction force relies on the exhaust volume and length.**

***Index Terms*—Soft sensors and actuators, hydraulic/pneumatic actuators, mechanism design, extendable and contractable actuator, inflatable structure.**

I. Introduction

UNLIKE conventional rigid actuators, soft actuators are known for their lightweight and high adaptability. These characteristics are attributed to the flexibility of the driving source, such as a wire or air, and the flexibility of the material used in the structure of the actuator, such as a plastic film or rubber. Therefore, soft actuators are suitable for telescopic and bending motions of multiple continuum bodies and are widely applied in manipulation [1]–[3] and wearable devices [4], [5].

Characterized by their lightweight [6], pneumatic artificial muscles (PAMs), referred to as McKibben actuators, are a type of pneumatic actuators that are widely used in biomimetic manipulators and exoskeletons. The McKibben actuator comprises a rubber tube covered with a flexible braided mesh shell. Here, the inflation and contraction occur by pressurizing the rubber tube [7], [8]. The McKibben actuator outputs a high contraction force despite its light weight; however, its contraction rate is not sufficiently high. Doi et al. [9] reported that the maximum contraction rate without a load was approximately 23.7%.

Other types of PAMs, such as the eversive PAM, which is based on the eversion principle of conventional McKibben's actuators [10], and pleated PAMs, which have pleats and improve the braided design of McKibben actuators [6], [11], have also been developed. Most of these actuators are designed to focus on the contracting motion; therefore, only a few of them can be used to generate the extending motion. Several foldable soft actuators with high extension rates have been proposed [12]–[17]. An extensible pneumatic actuator with bellows was proposed by Yukisawa et al. [12], [13], which comprised an inner rubber tube and outer bellows. The bellows suppress the expansion in the radial direction, thereby extending in the longitudinal direction when the rubber tube is pressurized. Owing to the high extension rate of the bellows, these actuators exhibit a high contraction rate of 476% (length/initial length), which is difficult to be achieved by conventional McKibben actuators, whose maximum contraction force reaches 250 N. As these actuators are designed to generate contracting motions rather than extending motions, they require external forces to be extended. Although both extending and contracting motions are required to realize telescopic motions in soft actuators, most soft actuators have not yet been designed to generate self-extending motions. A few soft inflatable actuators have been proposed to generate longitudinal self-extension [18]–[23]. Some have been proposed as growing structures rather than as soft actuators. These actuators comprise plastic film tubes that can be compactly stored. They generate an extending motion by inflating the tubes and realize a high extension rate; however, most of them are not designed to generate a contracting motion. A few actuators have realized both extending and contracting motions [17], [20]. Hammond et al. [20] proposed a pneumatic

Manuscript received: August 13, 2023; Revised: November 13, 2023; Accepted: December 6, 2023. This work was recommended for publication by Yong-Lae Park upon evaluation of the Associate Editor and Reviewers' comments. This work was supported by Fluid Power Technology Promotion Foundation, JST, JSPS KAKENHI (Grant numbers 19H01130, 21J20587, 21H05055, and 23H03443), and in part by the Waseda University for Special Research Projects (Grant number 2020R-071).

[1]Yasuka Tago is with the Graduate School of Creative Science and Engineering, Waseda University, Tokyo 169-8555, Japan (e-mail: uvh2025metro@asagi.waseda.jp). [2]Yuki Satake is with the Graduate School of Creative Science and Engineering, Waseda University, Tokyo 169-8555, Japan (e-mail: yuki.sa417@toki.waseda.jp). [3]Hiroyuki Ishii is with the Department of Modern Mechanical Engineering, and with Human Robotics Institute (HRI), Waseda University, Tokyo 169-8555, Japan (corresponding author; e-mail: hiro.ishii@waseda.jp).

Digital Object Identifier (DOI): see top of this page.

actuator that could generate both extending and contracting motions using an inflatable tube stored on a reel and an embedded spring. This actuator can be used to realize lightweight deformable structures; however, more powerful and well-controlled actuators are required.

Therefore, the objective of this study was to establish a novel inflatable design for soft actuators capable of extending and contracting. The proposed soft actuator comprises an inflatable tube with inner rings and uses a controllable stopper to store the tube. The combined motion between the tube with inner rings and the stopper can prevent buckling during extension (Fig. 1); buckling is a condition in which the tube snaps and becomes irreversible, blocking the flow path. The combined motion enables the inflated tube to generate a substantially longer and stiffer longitudinal extension than conventional inflatable tubes. Additionally, the contracting motion can be generated by the exhaust.

The remainder of this paper is organized as follows. Section II presents the principle and model of the proposed actuator, and Section III describes its mechanical design. The experimental evaluation of the performance of the actuator is presented in Section IV, and the corresponding results are discussed in Section V. Finally, the conclusions of the study are summarized in Section VI.

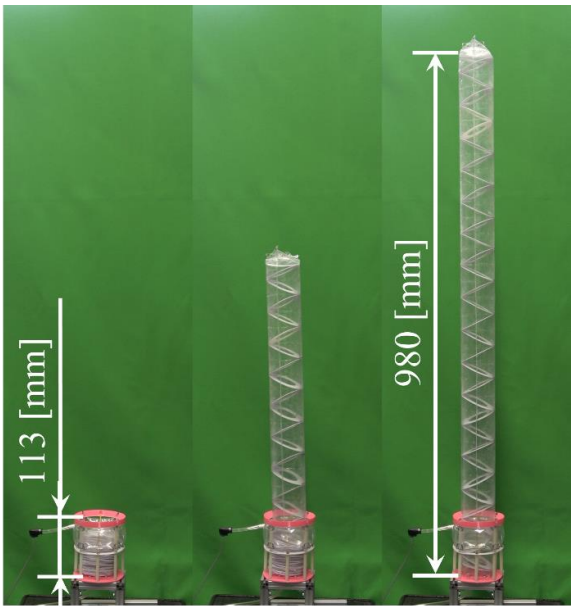

Fig. 1. Demonstration of the extending motion.

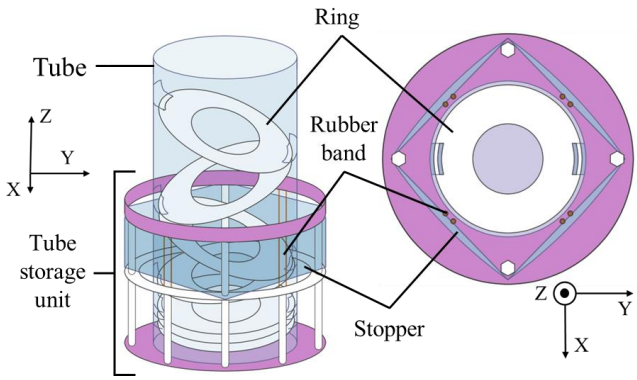

Fig. 2. Overview and cross-sectional view of the actuator when the stopper is off.

II. Principle and Model

This section introduces the principle and model of the actuator. The actuator comprised an inflatable tube with inner rings and a tube storage unit with stoppers (Fig. 2). The tube and stopper were inflated by filling them with air and deflating them by releasing the air. Oval plates (rings) with a hole in the center were arranged inside the tube in a zigzag pattern.

A. Principle of Actuation

Fig. 3 and Table I present the extending motion details. The tube is initially folded in the tube storage unit and begins to extend when pressurized. Pressurizing the stopper causes it to inflate (the stopper is on), and the stopper restricts the tube; therefore, the extension pauses temporarily. However, the stopper loosens at atmospheric pressure (the stopper is off) and resumes extension. The tube is gradually extended from the tip by switching the stopper on and off. Preventing a rapid increase

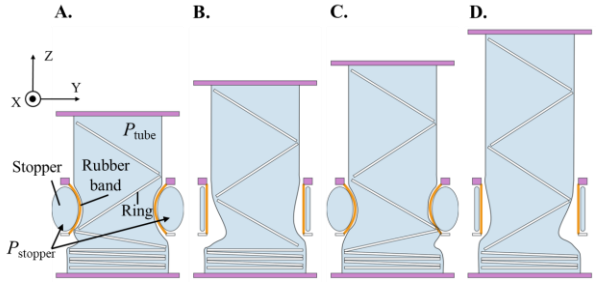

Fig. 3. Extending motion.

TABLE I
CONTROLLING THE PRESSURE DURING EXTENSION

Step	Stopper	$P_{stopper}$	P_{tube}
A	ON	High	High
B	OFF	Atmosphere	High
C	ON	High	High
D	OFF	Atmosphere	High

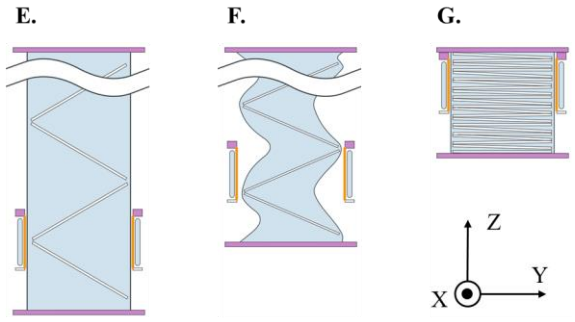

Fig. 4. Contracting motion.

TABLE II
CONTROLLING THE PRESSURE DURING CONTRACTION

Step	Stopper	$P_{stopper}$	P_{tube}
E	OFF	Atmosphere	Negative
F	OFF	Atmosphere	Negative
G	OFF	Atmosphere	Negative

in tube volume prevents excess reduction of pressure inside the tube (Ptube). Maintaining the pressure is important because the strength of an inflatable beam relies on internal pressure [24].

Fig. 4 and Table II present the contraction process. The tube contractions fold along the rings by depressurizing the tube with exhaust. The stopper should be at atmospheric pressure to ensure that the tube passes through the stopper.

B. Model of Contraction Force

The contraction force (F_{contract}) denotes the sum of the forces acting on the bottom of the actuator (F_1) and the tension force generated by the tension of the film (F_2). The film is attached to the bottom in two places on the left and right; therefore, F_2 is the sum of F_{2R} and F_{2L} (Fig. 5).

$$F_{\text{contract}} = F_1 + F_{2R} + F_{2L} = F_1 + F_2. \quad (1)$$

F_1 and F_2 can be attributed to the difference between the inside pressure (P_{tube}) and outside pressure ($P_{\text{atmosphere}}$) of the tube. F_1 is generated by the pressure applied to the bottom of the actuator; it depends on the base area (S_{base}) and P_{tube}.

$$F_1 = S_{\text{base}}\left(P_{\text{atmosphere}} - P_{\text{tube}}\right) \quad (2)$$

F_2 is generated by the pressure applied to the side of the actuator; it depends on P_{tube} (Fig. 6). F_2 is expressed as follows with the coefficient k_i:

$$F_2 = \sum (F_{2Ri} + F_{2Li}) = \sum k_i \left(P_{\text{atmosphere}} - P_{\text{tube}}\right). \quad (3)$$

Therefore, F_{contract} depends on P_{tube}.

$$F_{\text{contract}} = \left(S_{\text{base}} + \sum k_i\right)\left(P_{\text{atmosphere}} - P_{\text{tube}}\right) \quad (4)$$

Considering a considerably short time Δt, the change in F_{contract} ($\Delta F_{\text{contract}}$) is proportional to the change in P_{tube} (ΔP_{tube}).

$$\Delta F_{\text{contract}} = -\left(S_{\text{base}} + \sum k_i\right)\Delta P_{\text{tube}} \quad (5)$$

The tube volume depends on C_{length}, which indicates the ratio of the tube length (L_{tube}) to the maximum tube length ($L_{\text{tube-max}}$). The larger the volume, the lower is the pressure drop.

$$C_{\text{length}} = L_{\text{tube}}/L_{\text{tube-max}} \quad (6)$$

Therefore, when the exhaust volume is constant, as C_{length} increases (the tube volume increases), ΔP_{tube} decreases.

Assuming a constant C_{length}, that is, when the tip is fixed and the tube length is constant, the actuator during contraction can be divided into three states depending on the state of the film and the characteristics of the vacuum pump used for the exhaust.

State 1: The film collapses and the internal volume decreases. As the constant exhaust rate and tube volume decrease, P_{tube} decreases at an accelerated rate and F_{contract} increases at an accelerated rate.

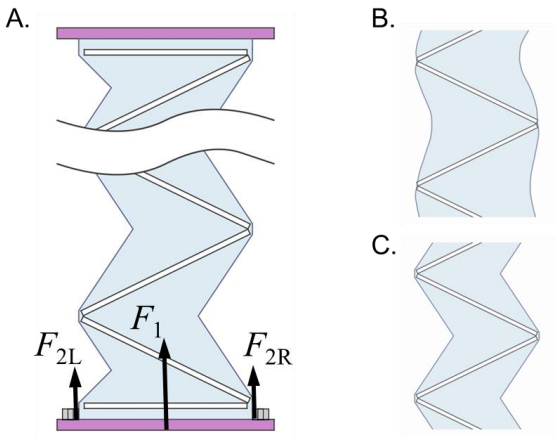

Fig. 5. **A**. Forces acting during contraction. **B**. The film is relaxed and moving in state 1. **C**. The film is strained and motionless in states 2 and 3.

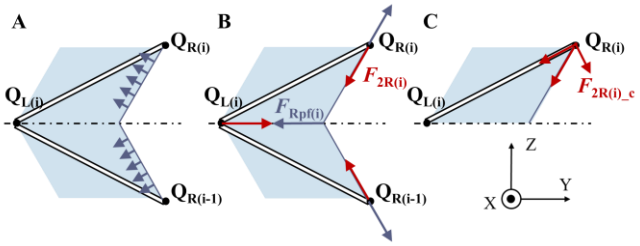

Fig. 6. Tension force generated by the tension in the film. **A**. Pressure differences between inside and outside of the tube generates pushing force on the film (blue arrows). **B**. Pushing force on the film induces tension forces on the film; hence, the rings are pulled by the tension force $F_{\text{Rpf(i)}}$. **C**. Tension force is resolved to two force components, and $F_{\text{2R(i)\_c}}$ generates moment to close the rings.

State 2: The film stops, and tension acts on it. Because the exhaust rate and tube volume are constant, ΔP_{tube} and $\Delta F_{\text{contract}}$ remain constant. Therefore, P_{tube} drops proportionally and F_{contract} increases proportionally.

State 3: The exhaust speed decreases as the vacuum pump approaches the ultimate vacuum pressure. As P_{tube} approaches the ultimate vacuum pressure ($P_{\text{tube-min}}$), ΔP_{tube} converges to zero and F_{contract} converges to the maximum contraction force ($F_{\text{contract-max}}$). However, as F_2 increases, ring deformation or tube damage may occur. Therefore, the F_{contract} at this point denotes the actual maximum contraction force.

III. Mechanical Design

Fig. 7 depicts an overview of the actuator during extension. The maximum and minimum tube lengths were 980 and 111 mm, respectively. The tube diameter was 64 mm, and the tube weighed 191 g excluding the air supply tube. The tube and stopper were composed of a plastic film laminated with nylon and polyethylene. This film can be easily heat-welded and exhibits adequate strength [23]; therefore, it was processed to produce a tube and stopper. Thin rings were attached to the tube using the same film. The rings and other parts of the stopper were fabricated using polylactic acid and a three-dimensional printer.

The tube must be collapsible along the length during

contraction and should not buckle during extension. Rubber bellows are an example of an inflatable structure that contract in the length direction. However, increasing the length is difficult because of the heaviness and buckling tendency of the material owing to the folds of the bellows. Therefore, we used a plastic film as the tube material and placed the rings inside as the inner frame. Accordingly, the tube was lightweight, and the folds were smooth when filled with air, thereby reducing the tendency of buckling. Additionally, the rings prevented radial collapse and induced contractions along the length. The rings were oval with a circular hole in the center, long diameter of 70 mm, and short diameter of 63 mm. The tube length per ring was 30 mm during extension.

The stopper is necessary to maintain the extension of the tube in the ON state and not interfere with the tube's extension or contraction in the OFF state. The plastic film used for the tube was incorporated into the stopper as well. Furthermore, rubber bands were placed between the stopper and tube to prevent slipping and ensure that the stopper does not interfere with the tube.

The stopper was operated using a 3-port solenoid valve (AIR VALVE 100EI, KOGANEI), and the tube was operated by switching the flow channel using two manual valves (Fig. 8). A compressor (EC1245H3, Hitachi Koki) was connected to two air tanks, and the pressure was regulated via a regulator and supplied to the tube and stopper separately. The solenoid valve was operated using pulse signals from the MCU (STM32); high-pressure air and atmospheric pressure air were provided alternately.

IV. Experiments

A. Extending Motion

Setup and Method: The extension performance was experimentally evaluated with time that is the pulse length when stopper was on ($t_{\text{pressurized}}$) and a certain load applied to tip (M_{tip}). Initially, the tube was contracted to its minimum length, a stopper was applied, and the tube was subjected to atmospheric pressure. Subsequently, the stopper cycle and pressurization of the tube were simultaneously initiated, extending until the tube reached its maximum length or buckled.

The stopper cycle was alternated between high pressure (approximately 20 kPa) and atmospheric pressure; the atmospheric pressure state lasted for 200 ms with $t_{\text{pressurized}}$ = 250, 500, and 1000 ms. The value of P_{tube} was set to 2.7 kPa when the tube was filled. The actuator was extended under two conditions of tip load, namely, M_{tip} = 0 and 30 g. Both P_{tube} and $L_{\max}$ were recorded, and the maximum length was achieved without buckling.

Results: As indicated in Fig. 9, the larger the value of $t_{\text{pressurized}}$, the longer the $L_{\max}$. In all cases with M_{tip} = 0, the actuator extends to the maximum length without buckling.

Fig. 10 indicates that P_{tube} increases when the stopper is in a high-pressure state and decreases when the stopper is in the atmospheric pressure state. The waveform with respect to $t_{\text{pressurized}}$ = 1000 ms verifies that the pressure inside the tube gradually increases, and this increase decelerates when the stopper is pressurized. This suggests that P_{tube} gradually converges as the stopper is continuously in a high-pressure state. This pattern was not observed when $t_{\text{pressurized}}$ = 250 ms because of the short pressurizing time. When the stopper was on, the volume in the tube remained constant and P_{tube} increased. As P_{tube} was high and remained stable when the stopper continued to remain in the ON state, we inferred that if $t_{\text{pressurized}}$ was longer than a certain value, P_{tube} can be sufficiently high to prevent buckling.

The behavior of P_{tube} can be divided into four steps (Fig. 11, Fig 12): (a) Before starting the stopper cycle and pressurization, a lag exists between the start of the compression and the actual start of the extension. (b) When extension begins, the pressure inside the tube is initially low before stabilizing gradually. (c) Once buckling occurs, the extension stops. (d) Finally, P_{tube} increases.

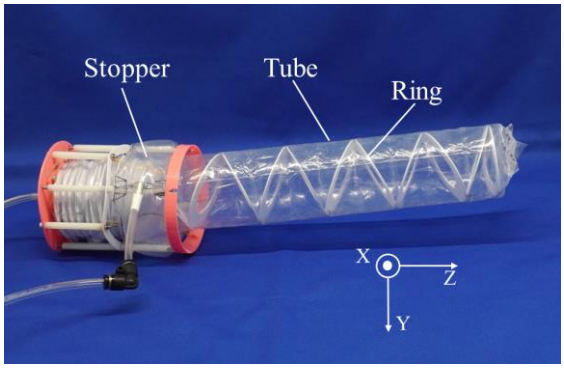

Fig. 7. Overview of the actuator.

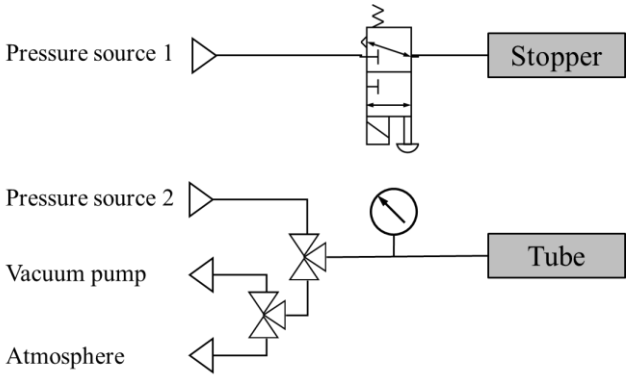

Fig. 8. Pneumatic system of the actuator.

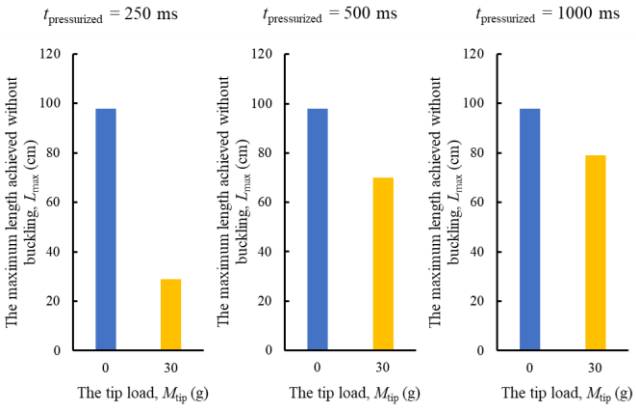

Fig. 9. Maximum length with respect to time ($t_{\text{pressurized}}$) and tip load (M_{tip}).

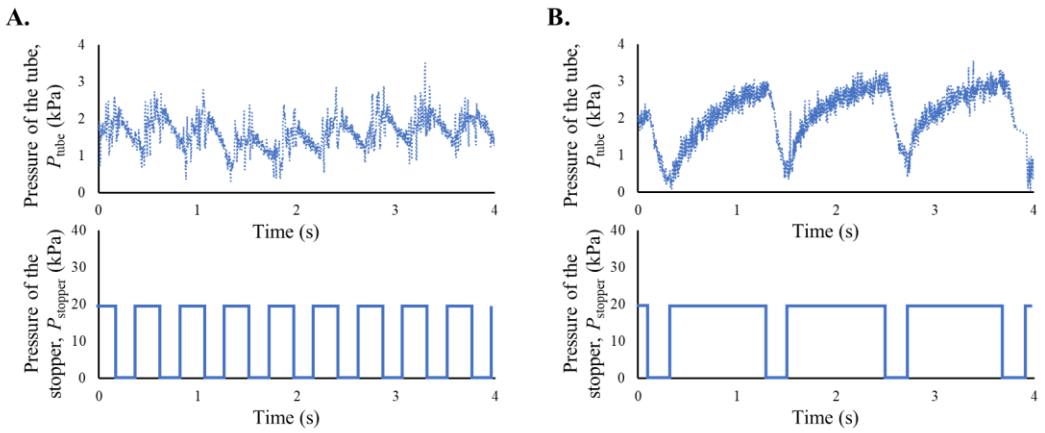

Fig. 10. Status of the stopper and the waves of P_{tube} transition at different values of $t_{pressurized}$ with M_{tip} set to 0 g. The moving-average method is applied for 10-s intervals. **A.** $t_{pressurized}$ = 250 ms. **B.** $t_{pressurized}$ = 1000 ms.

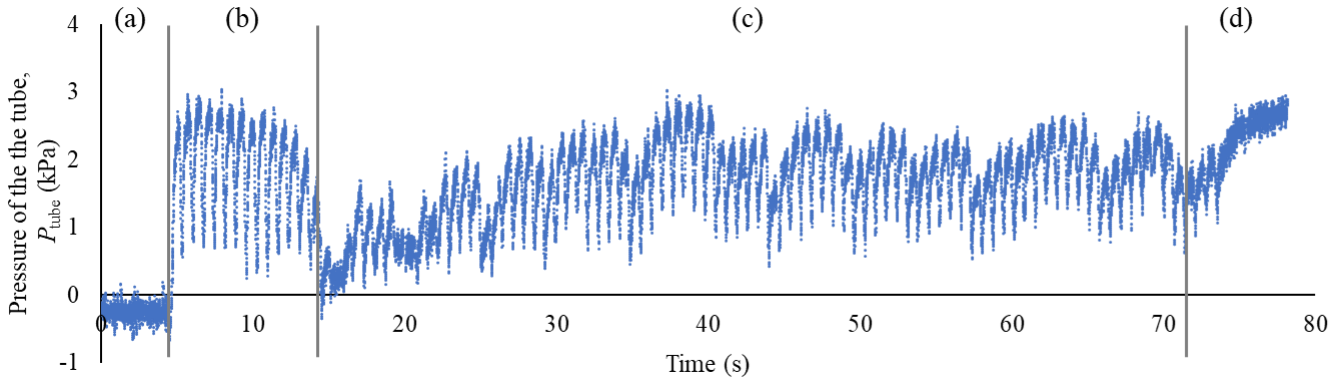

Fig. 11. P_{tube} transition with $t_{pressurized}$ = 500 ms and M_{tip} = 30 g. The moving-average method is applied for 30-s intervals.

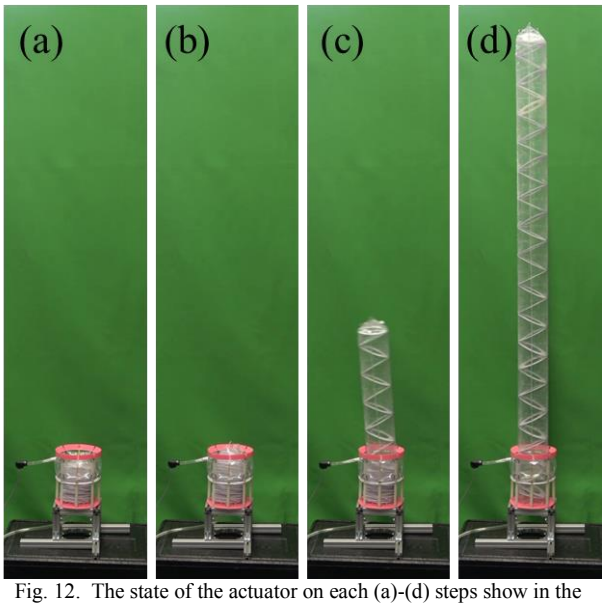

Fig. 12. The state of the actuator on each (a)-(d) steps show in the demonstration.

B. Contracting Motion

1) Set Length

Setup and Method: The contracting performance was experimentally evaluated by changing the specific length (C_{length}) and exhaust time ($t_{exhaust}$). One end of the actuator was fixed, and the other end was attached to a force gauge to ensure that no tension was applied at atmospheric pressure. The actuator was then exhausted, and $F_{contract}$ was calculated using a pressure gauge until the ring or the fixed film was deformed. Using one specimen, six trials were executed, each with C_{length} = 0.2, 0.3, 0.4, 0.5, 0.6, 0.7, 0.8, 0.9, and 1.

Results: Fig. 13 indicates that $F_{contract}$ increases depending on the total exhaust volume. Fig. 14 depicts the extracted graph at C_{length} = 0.5, which is a typical transition. This verifies that the tube can be divided into three states. In states 1, 2, and 3, $F_{contract}$ increases rapidly, $F_{contract}$ is linearly proportional to $t_{exhaust}$, and $F_{contract}$ approaches convergence, respectively. Except for the condition of C_{length} = 0.1 (Fig. 13), this trend is evident under other conditions. The smaller the C_{length}, the shorter the time required for each state. This is because a smaller C_{length} results in a larger change in P_{tube} with respect to the exhaust volume owing to the smaller tube volume. When C_{length} = 0.1, the tube exhibits minimum length, and $F_{contract}$ remains small. Additionally, ring deformations begin at a small $F_{contract}$ under large C_{length} conditions.

2) Set Force

Setup and Method: The maximum load ability of the actuator was evaluated by measuring the strain (ε) on setting the bottom load (M_{bottom}). ε is expressed as follows:

$$\varepsilon = (L_{tube-max} - L_{tube})/L_{tube} = (1 - C_{length})/C_{length}. \quad (7)$$

The tip of the actuator was fixed to the ceiling, and a load was suspended at the bottom of the actuator. The actuator was exhausted, and the contraction length (the difference between L_{tube} and $L_{tube\text{-}max}$) was measured. Using one specimen, six trials were executed, each with M_{bottom} = 0, 500, 1000, 1500, 2000, 2500, and 3000 [g].

Results: Fig. 15 indicates that the actuator fully contracted up to the minimum possible design length with M_{bottom} = 0, 500, and 1000 [g]. With M_{bottom} larger than 1500 [g], ε decreased as M_{bottom} increased and the rings bended. The deformation of the rings became more significant as M_{bottom} increased, and L_{tube} at contraction increased owing to gaps between the rings. However, after the contraction with M_{bottom} = 3000 [g], the actuator could be fully contracted with no load, that is, the actuator was not damaged even if M_{bottom} = 3000 [g].

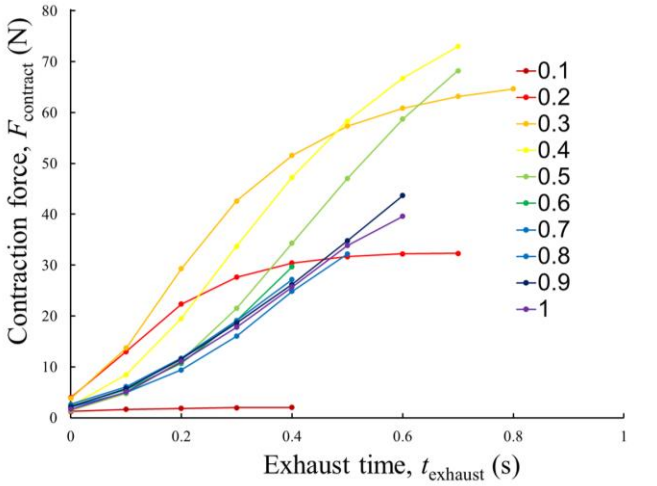

Fig. 13. Relationship between $F_{contract}$ and $t_{exhaust}$ for each C_{length} condition. The plots indicate the average of $F_{contract}$ over six trials for each $t_{exhaust}$ and C_{length} condition. The number of plots is aligned to the least number of plots under each C_{length} condition. All the results are presented for one specimen.

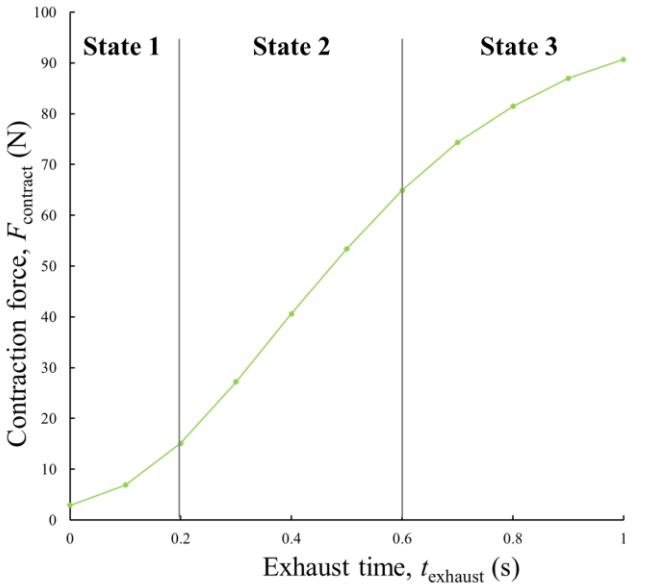

Fig. 14. Typical sample with C_{length} = 0.5.

V. Discussion

A. Extending Motion

Owing to the combined motion between the tube with inner rings and the stopper, the proposed soft actuator reached a height of 980 mm by a vertical extension, as depicted in Fig. 9. It also reached a height of 790 mm by a vertical extension with a 30 g weight at the tip. The results illustrated in Fig. 10 confirm that the stopper, which holds and releases the tube, contributes significantly to the extension. When the stopper holds the tube to maintain a constant volume, the internal pressure of the tube increases, thereby increasing the stiffness of the inflated tube. When the stopper releases the tube for extension, the pressure in the tube immediately decreases owing to an increase in its volume. As the stiffness of the inflatable tube decreases with a decrease in the pressure inside the tube, the duration of release, which can be controlled by the pressure in the stopper, should be sufficiently short to avoid buckling caused by the low pressure inside the tube. The results further verify that the extending length of the soft actuator can be controlled by regulating the number of releases, similar to that in stepper motors.

Certain similarities were observed when the extending motions of the proposed soft actuator and those of inflatable growing robots [18]–[23] were compared. In growing robots, the inflatable tube is stored before inflation and is gradually fed for the extending motion with the inner pressure maintained sufficiently high to avoid buckling. Reels are placed at the tip of an inflatable tube and are often used for tube feeding. The stopper and inner rings of the tube in the proposed soft actuator play a role similar to that of the feeder in growing robots. The difference lies in the position of the feeding mechanism, which is set at the end of the tube in the proposed soft actuator, whereas the mechanism is set at the tip of the tube in growing robots. Because of this design, the tip of the proposed soft actuator is substantially simpler and lighter than that of growing

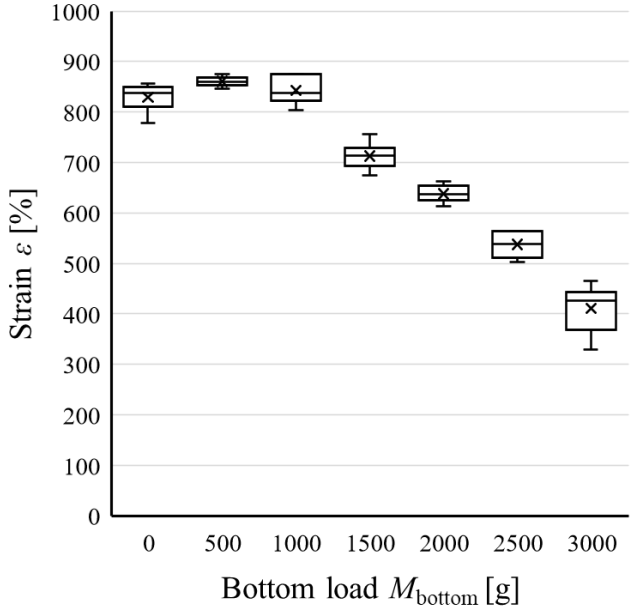

Fig. 15. Strain ε with respect to the bottom load M_{bottom}.

robots. Therefore, functional mechanical parts can be placed at the tips of the proposed soft actuators.

In Figs. 10 and 11, the pressure waveforms in the tube appear triangular with each valley representing the release motion of the stopper. As described in Section III, the tube extends by a length equal to the size of the ring in the tube with a single release motion of the stopper. Therefore, the length of the soft actuator can be estimated using the number of release motions of the stopper and the size of the ring, provided that the stopper releases only one ring via a single release motion (Fig. 11(c)). When buckling occurs owing to an excessive load at the tip or the tube is completely extended, the soft actuator cannot be extended further; therefore, the length cannot be estimated from the number of release motions. This situation is similar to the loss of steps in stepper motors and can be avoided by using the soft actuator in an acceptable range of load and length, which is often used to control the stepper motors. In this case, P_{tube} continues to increase because the volume remains constant (Fig. 11(d)). This situation can be easily detected by measuring P_{tube} using a pressure sensor.

The speed of the extending motion depends on the pressure in the tube and stopper, and a trade-off exists between the speed and stiffness. The longer the stopping time, the more stable the pressure in the tube and the slower the extension speed. A higher speed can be achieved by increasing the pressure applied to the tube if tougher films are used to fabricate the tube and a stopper is reinforced. The same factors can facilitate the increase in stiffness as well.

B. Contracting Motion

We confirmed that the proposed actuator can generate a contracting motion and force upon exhaustion. The contraction force increased with the exhaust volume. The maximum contraction force reached 73 N in an average of six trials with a C_{length} of 0.4, which was stronger than that of the reel actuator [20]. The maximum contraction ratio was 870%, which is higher than that of the McKibben actuator. The actuator can fully lift loads up to 1000 [g], and a strain of at least 300 % is exerted on it for loads up to 3000 [g]. This was achieved because of the ring inside the tube and the shape of its storage. Owing to the hole at the center of the rings, the air is smoothly exhausted from the tip to the end via decompression during the contracting motion. Additionally, the rings interact with the storage and induce organized folding in the longitudinal direction during contraction without circumferential collapse. After contraction, the tube returns to its initial shape during storage. Therefore, the soft actuator can extend again after complete contraction and repeat these extending and contracting motions.

The tube state model was validated and it could be applied until the exhaust continued and the ring began to deform. The endpoints of the graphs for each C_{length} condition (Fig. 14) were either in state 2 or state 3. In these states, the tube was at its minimum volume under the C_{length} condition (Fig. 5(c)). This indicated that ring deformation occurred when the film was under tension, validating the model in state 1. During actual contractions, the length of the tube gradually shortens, which in turn decreases the C_{length}. This implies that by retaining the exhaust volume in state 1 at each length, contraction can be achieved without breaking the soft actuator. Even though elastic deformations were observed on the rings, the actuator kept its initial contraction performance after it lifted a load of 3000 [g] for 6 times, as described in chapter IV. Therefore, we consider that the actuator can be used repeatedly if loads on the actuator is less than 3000 [g]. Moreover, the contraction force can be controlled by changing the amount of exhaust according to the model described in Section II. The controllability of the contraction force can be advantageous for the proposed soft actuator when compared with the growing robot, which generates the contracting motion using the constant force generated by a spring.

C. Expected Application

Only a few actuators, including ours, can perform both extending and contracting motion [17], [20]. Our actuator is characterized by being longer than those utilizing folding structures [17] and exerting a strong contraction force than growing robots [20].

Utilizing these characteristics as well as a high contraction rate and the ability to attach some functional parts on its tip, the actuator can be used as a manipulator. We are currently developing a self-lifting robot using the proposed actuator with a soft gripper to grab objects at its tip. This robot can grasp a beam from the ceiling by extending its motion and lifting its body, which includes a payload, via a contracting motion. The robot can replace large lifts if used for transportation, such as for transporting small items to high storage spaces at distribution centers. Moreover, by attaching cameras and sensors to the tip, the robot can be used for inspecting high places, such as for crack inspection of building envelopes.

VI. Conclusion

A design method was proposed for a novel pneumatic longitudinal actuator to perform both extending and contracting motions. A prototype developed using this method was experimentally evaluated. The analysis confirmed the effectiveness of the proposed design with respect to the tube with rings and the storage with the stopper. Based on the results, certain ideas regarding the control of the proposed soft actuator were proposed. A self-lifting robot is currently under development using the proposed design with a soft gripper on its tip. Future studies are planned to model and optimize the parameters during contraction.

References

[1] W. McMahan, V. Chitrakaran, M. Csencsits, D. Dawson, I. D. Walker, B. A. Jones, M. Pritts, D. Dienno, M. Grissom, and C. D. Rahn, "Field trials and testing of the OctArm continuum manipulator," in *Proc. 2006 IEEE Int. Conf. Robot. Autom.*, 2006. ICRA 2006., Orlando, FL, USA, pp. 2336–2341.

[2] N. Giri and I. Walker, "Continuum robots and underactuated grasping," *Mech. Sci.*, vol. 2, pp. 51–58, Feb. 2011.

[3] F. Renda, M. Giorelli, M. Calisti, M. Cianchetti, and C. Laschi, "Dynamic model of a multibending soft robot arm driven by cables," in *IEEE Trans. Robot.*, vol. 30, no. 5, pp. 1109–1122, Oct. 2014.

[4] H. In, B. B. Kang, M. Sin, and K. J. Cho, “Exo-glove: A wearable robot for the hand with a soft tendon routing system,” *IEEE Robot. Autom. Mag.*, vol. 22, no. 1, pp. 97–105, Mar. 2015.

[5] M. Wehner, B. Quinlivan, P. M. Aubin, E. Martinez-Villalpando, M. Baumann, L. Stirling, K. Holt, R. Wood, and C. Walsh, “A lightweight soft exosuit for gait assistance,” in *2013 IEEE Int. Conf. Robot. Autom.*, Karlsruhe, Germany, pp. 3362–3369.

[6] F. Daerden and D. Lefeber, “Pneumatic artificial muscles: actuators for robotics and automation,” *Eur. J. Mech. Environ. Eng.*, vol. 47, no. 1, pp. 11–21, Mar. 2002.

[7] C. P. Chou and B. Hannaford, “Measurement and modeling of McKibben pneumatic artificial muscles,” *IEEE Trans. Robot. Autom.*, vol. 12, no. 1, pp. 90–102, Feb. 1996.

[8] B. Tondu and P. Lopez, “Modeling and control of McKibben artificial muscle robot actuators,” in *IEEE Control Syst. Mag.*, vol. 20, no. 2, pp. 15–38, Apr. 2000.

[9] T. Doi, S. Wakimoto, K. Suzumori, and T. Kanda, “Research on bundle mechanism of thin McKibben artificial muscles -lst report: static characteristics of contraction ratio and contraction force,” in *Proc. 2015 ISME Conf. Robot. Mechatron.*, pp. 1P1-B03_1–1P1-B03_4, 2015.

[10] T. A. Abrar, F. Putzu, J. Konstantinova and K. Althoefer, “EPAM: Eversive pneumatic artificial muscle,” in *2019 2nd IEEE Int. Conf. Soft Robot. (RoboSoft)*, Seoul, Korea (South), Apr. 14, 2019, pp. 19–24.

[11] F. Daerden, D. Lefeber, B. Verrelst, and R. Van Ham, “Pleated pneumatic artificial muscles: compliant robotic actuators,” in Proc. 2001 IEEE/RSJ Int. Conf. Intell. Robots Syst., Expanding the Societal Role of Robotics in the Next Millennium (Cat. No.01CH37180), Maui, HI, USA, Oct. 29, 2001, vol. 4, pp. 1958–1963.

[12] T. Yukisawa, Y. Ishii, S. Nishikawa, R. Niiyama, and Y. Kuniyoshi, “Modeling of extensible pneumatic actuator with bellows (EPAB) for continuum arm,” *2017 IEEE Int. Conf. Robot. and Biomim. (ROBIO)*, Macau, Macao, Dec. 5, 2017, pp. 2303–2308.

[13] T. Yukisawa, S. Nishikawa, R. Niiyama, Y. Kawahara, and Y. Kuniyoshi, “Ceiling continuum arm with extensible pneumatic actuators for desktop workspace,” in *2018 IEEE Int. Conf. Soft Robot. (RoboSoft)*, Livorno, Italy, Apr. 24, 2018, pp. 196–201.

[14] E. W. Hawkes, D. L. Christensen, and A. M. Okamura, “Design and implementation of a 300% strain soft artificial muscle,” in *2016 IEEE Int. Conf. Robot. Autom. (ICRA)*, Stockholm, Sweden, May 16, 2016, pp. 4022–4029.

[15] F. Maghooa, A. Stilli, Y. Noh, K. Althoefer, and H. A. Wurdemann, “Tendon and pressure actuation for a bio-inspired manipulator based on an antagonistic principle,” in *2015 IEEE Int. Conf. Robot. Autom. (ICRA)*, Seattle, WA, USA, May 26, 2015, pp. 2556–2561.

[16] Y. Miao and F. Chen, “Shape optimization of soft pneumatic bellows for high energy density,” in *2021 27th Int. Conf. Mechatron. Mach. Vis. Practice (M2VIP)*, Shanghai, China, Nov. 26, 2021, pp. 480–485.

[17] R. V. Martinez, C. R. Fish, X. Chen, and G. M. Whitesides, "Elastomeric origami: programmable paper-elastomer composites as pneumatic actuators." *Adv. Funct. Mater.*, vol. 22, no. 7, pp. 1376–1384,Feb. 2012.

[18] T. Takahashi, K. Tadakuma, M. Watanabe, E. Takane, N. Hookabe, H. Kajiahara, T. Yamasaki, M. Konyo, and S. Tadokoro, “Eversion robotic mechanism with hydraulic skeleton to realize steering function,” *IEEE Robot. Autom. Lett.*, vol. 6, no. 3, pp. 5413–5420, Jul. 2021.

[19] J. H. Kim, J. Jang, S. M. Lee, S. G. Jeong, Y. J. Kim, and J. H. Ryu, “Origami-inspired new material feeding mechanism for soft growing robots to keep the camera stay at the tip by securing its path,” *IEEE Robot. Autom. Lett.*, vol. 6, no. 3, pp. 4592–4599, Jul. 2021.

[20] Z. M. Hammond, N. S. Usevitch, E. W. Hawkes, and S. Follmer, “Pneumatic reel actuator: Design, modeling, and implementation,” in *2017 IEEE Int. Conf. Robot. Autom. (ICRA)*, Singapore, May 29, 2017, pp. 626–633.

[21] E. W. Hawkes, L. H. Blumenschein, J. D. Greer, and A. M. Okamura, “A soft robot that navigates its environment through growth,” *Sci. Robot.*, vol. 2, no. 8, p. eaan3028, 2017.

[22] D. A. Haggerty, N. D. Naclerio, and E. W. Hawkes, “Hybrid vine robot with internal steering-reeling mechanism enhances system-level capabilities,” *IEEE Robot. Autom. Lett.*, vol. 6, no. 3, pp. 5437–5444, Jul. 2021.

[23] Y. Satake, A. Takanishi, and H. Ishii, “Novel growing robot with inflatable structure and heat-welding rotation mechanism," in *IEEE/ASME Trans. Mechatron.*, vol. 25, no. 4, pp. 1869–1877, Aug. 2020.

[24] R. L. Comer and S. Levy, “Deflections of an inflated circular-cylindrical cantilever beam.” *AIAA J.*, vol. 1, no. 7, pp. 1652–1655, Jul. 1963.